Egypt. J. Chem. **Vol. 67**, No. 2 pp. 527 - 541 (2024)

Egyptian Journal of Chemistry

http://ejchem.journals.ekb.eg/

Bioremediation of Congo red Dyes using Biosynthesized copper\iron Nanoparticles

Mai Taha [1*], Mohammed Abbas [1], Elham M. Ali [2], Hala Fakhry [3,4], and Ashraf Elsayed [1]

[1] *Botany Department, Faculty of Science, Mansoura University, Egypt*

[2] *Department of Aquatic Environmental Science, Faculty of Fish Resources, Suez University, Egypt*

[3] *City of Scientific Research and Technological Applications, (SRTA-City), New Borg El-Arab City, P.O.Box 1121934, Egypt*

[4] *National Institute of Oceanography and Fisheries (NIOF), Cairo 11865, Egypt.*

Abstract

Water contamination by organic dyes and pathogenic bacteria has a negative impact on human health. Bimetallic nanoparticles are promising materials in water treatment. In the current study, a bimetallic of copper and iron nanoparticles (CuO/Fe_2O_3 NPs) was synthesized by the extract of *Fusarium oxysporum*. CuO/Fe_2O_3 NPs were characterized using different methods such as UV–Vis spectroscopy and transmission electron microscopy (TEM). The micrographs of TEM showed particle sizes ranging from 4-12 nm while UV–Vis analysis exposed the characteristic peak at 277 nm after the synthesis of CuO/Fe_2O_3 NPs. The antimicrobial activity of CuO/Fe_2O_3 NPs was tested against Gram +ve (*Streptococcus* sp, *Bacillus subtitles*), and Gram -ve (*E. coli*, *Salmonella typhi*) bacteria. The biosorption of Congo Red (CR) dye using the bio-synthesized CuO/Fe_2O_3 NPs was studied. The biosorption studies were investigated at different time intervals and different dye concentrations. The studies revealed that the bio-sorption percentage of 97.167 % was achieved only after 10 min of contact at 25 ppm. The maximum Langmuir isotherm adsorption capacity was 155.738 mg/g. For the kinetic studies, the bio-sorption process followed the pseudo-second-order model and it was involved in more than one single kinetic stage.

*Keywords:*Congo red removal; Bimetallic; CuO/Fe_2O_3 NPs; *Salmonella typhi*; *Streptococcus*; Adsorption equilbrium isotherms; Kinetic studies

1. Introduction

In recent years, the availability of clean water is the most pressing issue in our world [1-6]. Organic, inorganic, and biological pollutants infiltrate water bodies due to urbanization and industrialization, which is dangerous to the environment and human health. The main danger to human health is environmental pollution because it causes various diseases all over the world [7, 8].

Different industries like paper printing, food, cosmetics, and textile are playing a major role in producing organic dyes to water [9-12]. These industries discharge a large number of contaminants into the water bodies. When these contaminants are discharged into the aquatic environment it imperils the aquatic life by decreasing the oxygen amount which causes a great threat to human health [13-15]. Some of these industries use dyes, and as a result, a massive amount of colored wastewater is generated. The presence of dyes in water is highly visible and undesirable even at very low concentrations [16, 17]. The by-products that output from the degradation of organic dyes like synthetic azo dyes have harmful impacts on the environment. It contains toxic aromatic compounds and the elimination of these compounds through aerobic waste treatment are still low [18]. Congo red is an anionic dye that contains two azo groups.

The most public health concern is bacterial contamination of water as it causes many diseases. Organisms such as *Salmonella typhi* and *Escherichia coli* are transmitted through water and cause ill health

*Corresponding author e-mail maimohsentaha86@gmail.com; (Mai Taha)

Received date 26 May 2023; revised date 28 July 2023; accepted date 31 July 2023

DOI: 10.21608/EJCHEM.2023.213599.8030

in communities that consume water contaminated with the bacteria [18-22]. The antimicrobials like antibiotics and inorganic agents are playing a vital role in civil life [23, 24]. Trending different technological developments to vanquish this issue, nanotechnology is dominant in this situation. The antimicrobials like antibiotics and inorganic agents are playing a vital role in civil life [25]. Trending different technological developments to vanquish this issue, nanotechnology is dominant in this situation.

Nanotechnology is a promising area of science that has developed in the past 20 years in the nanoscience field. Nanoparticles (NPs) sizes are in ranging from 0 to 100 nm in diameter [26-28]. There is a great interest in nanoparticle synthesis and applications due to their magnetics, optics, electronics chemistry unique properties [29-32], that's why NPs have exhibited great potential in environmental remediation [33-35]. Green synthesis is a high-yield and eco-friendly path for nanoparticle preparation [36-38]. Fungi have powerful enzyme systems capable of mediating the biosynthesis of metal oxide nanoparticles [39-43]. The unique structure of NPs like shape, size, and lattice causes an increment in their applications [44-47]. Within the different NPs, metal oxide NPs are generally considered a secure material for humans and the environment [48, 49]. Recently, it has been found that CuO/Fe_2O_3 bimetallic nanoparticles enhance the elimination of pollutants because of the different potential inhibitory effects between CuO and Fe_2O_3 [50-52].

The dye removal by using bimetallic CuO/Fe_2O_3 nanoparticles occurs in two main ways: photocatalytic degradation and adsorption. The photocatalytic degradation ability of CuO/Fe_2O_3 for dyes has been reported, whereas, the adsorption of dyes onto bimetallic CuO/Fe_2O_3 NPs could be a viable topic. Various environmental factors can impact the adsorption process of wastewater such as pH, contact time, adsorbent dosage, stirring rate, and dye concentration [53].

Antibiotic-resistant bacteria withstand the inhibitory activity of an antibiotic to which it was initially sensitive [54, 55]. This occurs because of the uncontrolled use of antibacterial drugs in medicine. It causes due to the repeated exposure of bacteria to sub-lethal doses of antibiotics which results in their adaptation. This adaptation is due to the production of antibiotic degradation enzymes by bacteria [56]. Now nanoparticles are a new agent with a large surface area due to their small size, with physical and chemical properties which make them have a high capability in dealing with pathogen bacteria that can penetrate their cell wall [57].

In the present work, CuO/Fe_2O_3 nanoparticles were synthesized by a green method using fungal extract and characterized by X-ray diffraction (XRD), UV-Vis spectrophotometer, Fourier Transform Infra-Red Spectroscopy and Transmission Electron Microscopy (TEM). The biosynthesized CuO/Fe_2O_3 NPs were employed as an effective adsorbent for removing Congo red dye from the contaminated water.

2. 2. Experimental

2.1. Materials

Cupric Sulphate ($CuSO_4$), Ferric Sulphate ($FeCl_3$), and Congo red were purchased from Merck, Germany. *Fusarium oxysporum* was collected from the mycological lab at the Botany Department, Faculty of Science, Mansoura University. *Bacillus subtilis, Streptococcus sp, Salmonella typhi,* and *E. coli* strains were collected from the bacteriological lab at the Botany Department, Faculty of Science, Mansoura University.

2.2. Preparation of Congo red dye

The Congo red dye was used as a contaminant dye model in this study. A concentrated pure dye solution of 1000 ppm was prepared in which a specific amount of dye powder was dissolved in distilled water, and different concentrations of CR (25-250 ppm) were prepared through the dilution of the stock solution.

2.3. Biosynthesis of CuO\Fe$_2$O$_3$ nanoparticles by Fusarium oxysporum

Fusarium oxysporum [41, 43] was cultured on a PDA medium and then incubated at 25 ℃ and the culture of this fungus was maintained at 4℃ for use in the biosynthesis process [39]. *Fusarium oxysporum* biomass was obtained by growing the fungus on a PDA medium and forming agar discs, "5 discs" were added to 100 ml of a liquid medium called MGYP media (malt extract 3 g\l, yeast extract 3 g\l, dextrose 10 g\l and peptone 5 g\l and incubated in rotating shaking "130 rpm" for 72 hours at 26±2℃. After the incubation period, the fungal biomass was separated by filtration from the media, then washed three times

with sterile distilled water for removing the residues from the media. To each 100 ml of sterile de-ionized water, 20 g wet fresh weight of fungal biomass are immersed in 100 ml sterile de-ionized water and incubated at the same previous conditions for 24 hours, then the cell-free filtrate was prepared by removing the biomass using filtration and then was adjusted to pH 6, for each 100 ml of cell-free filtrate. Carefully weigh "$FeCl_3$, $CuSO_4$". making the final concentration of 5mM. These flasks were incubated in the previous condition under the dark condition to prevent photo-oxidation of metal ions. The resulting nanoparticles were dried in an oven at 60℃ for 48 hours the calcinated at 400℃ for 2 hours.

2.4. Characterization of CuO\Fe_2O_3 oxide nanoparticle

The formation of CuO/Fe_2O_3 NPs was detected by color changing of the reaction mixtures [40] and then scanned by UV visible spectrometry, using a (JENWAY UV vis spectrophotometer – UK) in the wavelength range 200-500 nm. The fungal extract was used as a blank sample. Transmission Electron Microscopy (TEM), X-ray Diffraction (XRD) Patterns, Fourier Transform Infra-Red (FT-IR) Spectroscopy analysis, and Selected Area Electron Diffraction (SAED) techniques were used for the characterization of CuO/Fe_2O_3 NPs. For detecting the shape and size of the myco-synthesized bimetallic nanoparticles, the CuO/Fe_2O_3 NPs suspension was dropped on a Gilder G200 TEM grid and dried, standard 200 square mesh, 3.05 mm diameter, and analyzed using JEOL JEM 2100 (HRTEM) operated at a voltage of 200 KV. SAED investigated the crystalline structure of the biosynthesized CuO/Fe_2O_3 NPs through the homogenous and the arrangement of the concentric diffraction ranges and extermination of crystalline planes. XRD, D8ADVANCE, Germany, was used to determine the atomic structure or the molecular structure of the NPs crystal. FT-IR Spectroscopy (Bruker VERTEX 80, Germany), a combined platinum diamond ATR, comprises a diamond disk as that of an internal reflector in the range 4000-400 cm-1 with resolution 4 cm-1, refractive index 2.4.

2.5. Evaluation of antimicrobial activity and Minimum Inhibitory Concentration (MIC) of the bio-synthesized CuO\Fe_2O_3 NPs

The antibacterial activity of myco-synthezied $CuO\backslash Fe_2O_3$ nanoparticles was evaluated against Gram-positive (*Bacillus subtilis; Streptococcus sp*) and Gram-negative (*Salmonella typhi; E. coli*) bacteria using well diffusion method. One loopful of pathogenic bacterial strains was cultivated on LB broth media (Tryptone 1, yeast extract 0.5, and sodium chloride 1 g\100 mL) and incubated at 37℃ for 24h. 10µL of the bacterial culture at OD_{600}= 1, inoculated on LB agar plates and swapped by using sterile cotton swap. One milligram of $CuO\backslash Fe_2O_3$ NPs was suspended in sterile deionized water and sonicated to provide a homogenized suspension, and then 50 µL were poured into a 9 mm diameter well made by a sterile cork borer. The plated were incubated at 37℃ for 24h, after incubation the inhibition zone was measured and recorded. MIC and dose-dependent were investigated by using the well diffusion method against the tested organisms at the concentrations of 0.25, 0.5, 0.75, 1.0, 2.0, and 3.0 mg\mL) of $CuO\backslash Fe_2O_3$ NPs on the 9 mm wells. The plates were incubated at 37℃ for 24h and after the incubation period, the inhibition zone was measured in millimeters.

2.6. Bio-sorption experiments

The physicochemical parameters' effects on the CR bio-sorption onto the bio-synthesized $CuO\backslash Fe_2O_3$ NPs, equilibrium, and kinetic studies were conducted in 250-mL Erlenmeyer flasks using 100 mL of a 50 ppm dye solution in a thermostatic shaking water bath (150 rpm). Kinetic studies were conducted using a constant amount of bio-synthesized NPs (0.1 g/L) and CR dye concentration (50 mg/L). The experiments were performed at different time intervals (5–120 min) and continued till equilibrium was reached. While Equilibrium isotherm studies were carried out at various concentrations of the used CR dye (25-250 mg/L), constant equilibrium time (10 min), and a constant amount of the bio-synthesized NPs (0.1 g/L). The next step is the centrifugation of the solutions from the bio-sorption experiments for 10 min at 10,000 rpm. After that, the maximum absorbance of the standard CR dye solutions before bio-sorption and the supernatant after it was measured using a UV–vis spectrophotometer at 498 nm. The bio-sorption

Removal percent (% R), and the bio-sorption capacity at equilibrium and at "t" time (q_e mg/g), (q_t mg/g), respectively were calculated according to Eqs. (1), [58], and [59, 60], respectively [59, 61]:

$$R\% = (C0 - Ce)/C0 * 100 \quad (1)$$

$$qe = \frac{(C_0 - C_{e)}}{M} * V \quad (2)$$

$$q_t = \frac{(C_0 - C_t)}{M} * V \quad (3)$$

where C_o (mg/L), C_e (mg/L), and C_t (mg/L) are the concentration of CR dye at initial, equilibrium, and "t" time, respectively; V (L) is the used dye solution volumes; M (g) is the used dose of the bio-synthesized CuO/Fe_2O_3 NPs.

2.7. Optimization of dye removal using the bio-synthesized CuO\Fe_2O_3 NPs.

The best operating conditions parameters for the removal process of CR bio-sorption were assessed by Response surface methodology (RSM), using central composite design (CCD) and Design-Expert version 13 software. The factors that affect the CR sorption involved four factors, namely the initial concentration of CR (ppm), NPs dosage (g\L), pH, and contact time (min) .

2.8. Phytotoxicity study

The toxicity study was investigated with degraded dye (Congo red) using the seeds of *Vicia faba* Sakha1. The seeds were washed to remove dust by wiping them with dist. H_2O. After that, they were surface sterilized using a 1.2% sodium hypochlorite solution. Ten seeds were soaked in treated water overnight before germination and watered with 5 ml of degraded dye per day. Positive control was set up with distilled water, while 10 ppm Congo red dye was used as a negative control for soaking and watering. Growth parameters were recorded after the emergence of radicals as an indicator for germination. The length of both radical (root) and plumule (shoot) besides the rate of germination was noticed after 1 week. The experiment was carried out at room temperature with three replicas.

3. Results and discussion

3.1. Biosynthesis of nanoparticles by Fusarium oxysporum

In this study, *Fusarium oxysporum* was grown in MGYP media and the growth was confirmed by color change of the media (Figure 1). CuO\$Fe_2O_3$ nanoparticles were synthesized by using a cell-free extract of the fungus which acts as a possible source of stabilizing and reducing agent for the reduction of copper and iron ions into CuO\$Fe_2O_3$ nanoparticles. The complete process of nanoparticles synthesis was confirmed by a change in color as shown in (Figure 2)

Figure (1): A) MGYP broth media, B) MGYP broth and *Fussarium oxysporum*

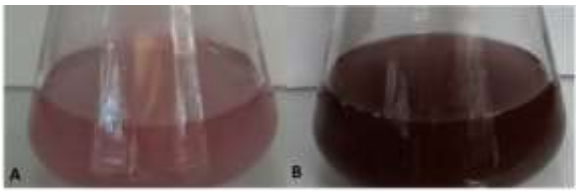

Figure (2): A) Cell-free extract, B) CuO\Fe_2O_3 nanoparticles

3.2. Characterization of the bio-synthesized CuO\Fe_2O_3 NPs

3.3. UV Spectroscopy:

The UV–Vis Spectrophotometer technique was used to confirm the presence of CuO\$Fe_2O_3$ nanoparticles in the prepared solution. The absorption peak was observed at 277 nm as shown (Figure 3) which revealed that the *Fusarium oxysporum* exhibits the CuO\$Fe_2O_3$ bimetallic NPs stable synthesis.

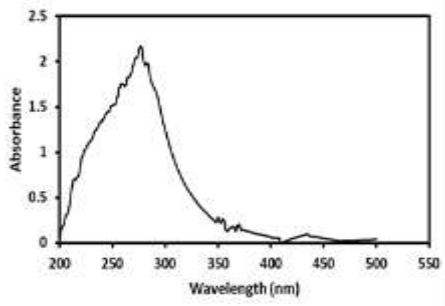

Figure (3): UV-vis spectrum of the bio-synthesized CuO\Fe_2O_3 nanoparticles.

3.4. XRD pattern analysis

The XRD pattern profile of $CuO\backslash Fe_2O_3$ nanoparticles is shown in Figure.4. The formation of bimetallic CuO/Fe_2O_3 NPs can be also confirmed through the appearance of the characteristic sharp bands in the XRD diffraction pattern identified in the Joint Committee on Powder Diffraction Standards JCPDS card no JCPDS 48-1548, 82-1533, and 24-1005 of CuO, Fe_2O_3 and their bimetallic compartment.

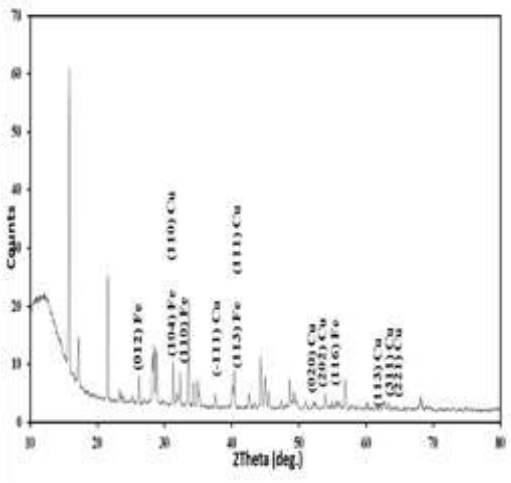

Figure (4): XRD spectrum of $CuO\backslash Fe_2O_3$ NPs

3.5. TEM Analysis

TEM analysis was investigating the morphology, shape, and size of nanoparticles. The TEM images show spherical-shaped supported nanoparticles over oxidized species the bio-synthesized $CuO\backslash Fe_2O_3$ NPs have a size of 18-36 nm. The crystallization of Fe_2O_3 is confirmed by the observed inter-planar of 4.34 and 5.97 nm. The selected area electron diffraction (SAED) Figure 5c confirmed The crystalline character of the bio-synthesized $CuO\backslash Fe_2O_3$ NPs, suggesting that they are polycrystalline structures due to The existence of a quasi-ring-like diffraction pattern.

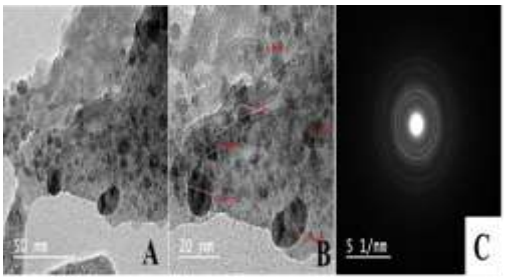

Figure (5): A- B TEM images of the bio-synthesized $CuO\backslash Fe_2O_3$ NPs and C) SAED Pattern of $CuO\backslash Fe_2O_3$ NPs

3.6. FTIR spectrum

To recognize the functional groups found in the biosynthesized $CuO\backslash Fe_2O_3$ nanoparticles, The formation of both bimetallic CuO/Fe2O3 nanoparticles can be observed through the formation of the vibration within the range of 3500-500 cm-1 in the FTIR optical transmittance spectra as shown in Fig. 6. Characteristic peaks observed at 597 and 1043 cm^{-1} were assigned to vibrations in CuO. The sharp peak at 3442.45 cm^{-1} is due to hydroxyl groups of water existence molecules. The broad band at 3361 cm^{-1} corresponds to O–H stretching within polyphenols or carboxylic acid [44]. In addition, the characteristic peaks at 1043 cm^{-1} can be attributed to C–H stretching of methyl group, C–O–H bending, and C–O stretching, respectively, all of which are compatible with plant polysaccharides. The capping components appear to be composed of amide, hydroxy groups, polysaccharides and carboxy, carboxylate, and/or ester moieties, according to the FTIR spectroscopic findings [45].

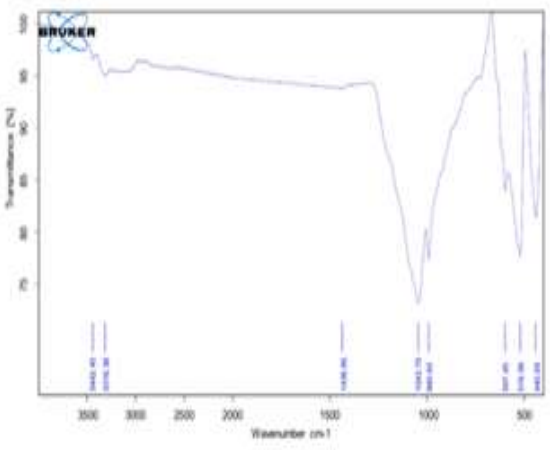

Figure (6): FTIR spectrum of the bio-synthesized $CuO\backslash Fe_2O_3$ NPs.

3.7. Antibacterial activity

The effect of NPs on *Bacillus subtilis*; *Streptococcus sp*; *Salmonella typhi* and *E. coli* were studied using well diffusion method. The zone of inhibition was observed in all plates which inferred that $CuO\backslash Fe_2O_3$ NPs have antimicrobial activities. MIC value of $CuO\backslash Fe_2O_3$ NPs was investigated as being 2mg\ml for *Bacillus subtilis* and *Salmonella typhi* and 3 mg\ml for *Streptococcus sp* and *E. coli*. The antimicrobial activity is mainly due to the generation of highly reactive species like OH^- and

O_2^{2+}. The OH^- and O_2^{2+} damage the cell membrane and cell wall from the outside. The antibacterial effect of NPs on the growth of bacterial strains is shown in Figure 7 where the values of the inhibition zone are presented in Table 1.

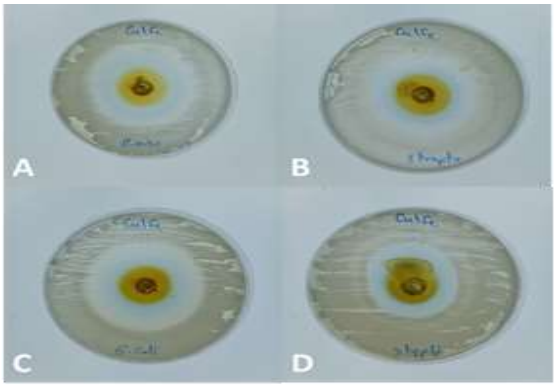

Figure (7): Antibacterial effect of mycosynthesized CuO\Fe_2O_3 nanoparticles.

Table 1: The inhibition zone values of CuO\Fe_2O_3 nanoparticles.

Bacteria	Inhibition zone (mm)					
NPs Concentration	0.25	0.5	0.75	1	2	3
Streptococcus sp	16	18	21	25	3	43
E. coli	N\C	18	20	28	3	42
Bacillus subtilis	15	23	27	31	35	46
Salmonella typhi	N\C	N\C	19	20	37	39

Note: N\C means no inhibition zone.

3.8. Kinetic Studies of Congo Red dye bio-sorption onto the biosynthesized CuO\Fe_2O_3 NPs.

The impact of contact time on the bio-sorption removal percentage (% R) at different intervals (5-120 min) was investigated and illustrated in Figure 8. The % R increased with increasing time until it reached equilibrium within 10 min, The biosynthesized CuO\$Fe_2O_3$NPs were able to bio-sorb 83% of CR dye molecules within the first 5 min of contact time, indicating the rapid affinity between bio-sorbate and bio-sorbent. As the bio-sorption process might be a time-consuming factor, all of the active sites were available and sufficient at the beginning of the bio-sorption process, but once equilibrium was reached, these sites began to be occupied by the CR dye molecules. A similar trend was reported in the adsorption of C.I. BR 14 dye on Cs/GP/VP/ A . donax beads[46].

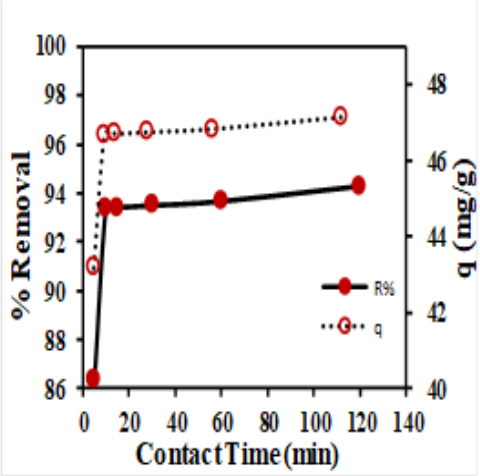

Figure (8): Effect of Contact time (min) on the bio-sorption of Congo Red onto the biosynthesized CuO\Fe_2O_3 NPs.

Important insights into the bio-sorption mechanisms, which may be governed by external or film diffusion, pore diffusion, and bio-sorption on the pore surface, or a combination of more than one step, are provided by bio-sorption kinetics [62, 63]. The four common kinetic models of pseudo-first order (PFO), pseudo-second-order (PFO), Elovich, and Intra-particle diffusion models were fitted to the obtained data to anticipate CR's bio-sorption process onto the bio-synthesized NPs, These models' corresponding equations are as follows:

$$\mathrm{Ln}\,(q_e - q_t) = \ln q_e - K_1 t \qquad (6)$$

$$\frac{t}{q_t} = \frac{1}{(K_2 q_e)2} \qquad (7)$$

Where q_t and q_e is the adsorbed CR amount at time t and at equilibrium (mg/g) respectively. k1 (min_1) is the first-order reaction rate constant, k_2 is the second-order reaction rate equilibrium constant (g/mg min), is the initial adsorption rate (mg/g min), and is the extent of surface coverage and activation energy for chemisorption (g/mg), the kid is the intra-particle diffusion rate constant, and c give a prediction about the boundary layer thickness.

The calculated ($q_{calculated}$) values of the first-kinetic model (PFO) differed from their experimental ones, meaning that this model was not appropriate enough to describe the bio-sorption process of CR dye.

According to the obtained Correlation coefficient (R^2), the pseudo-second order model (R^2 = 0.9998) is fitting better than the pseudo-first-order model (R^2 = 0.858), besides, the calculated value of bio-sorption capacity (q_e,cal= 3.415) was closer to the experimental (q_e, exp= 48.804) value in case of Pseudo-Second-Order model, implying that the CR dye molecules are chemically bio-sorbed (chemisorption)onto the bio-synthesized NPs. As the bio-sorption was chemisorption, the best model describing this process is the simple Elovich mode [64]. The obtained R^2 values indicate that the Elovich equation fitted the experimental data well; suggesting that the chemisorption process between the CR dye particles and the biosynthesized CuO/Fe_2O_3 NPs may include valence forces by sharing electrons between them [62, 63]. The intra-particle diffusion model was fitted to the experimental data to further explore the bio-sorption mechanism. The linearized graph in Fig. 9 and its kinetic parameters in Table 3, revealed that the biosynthesized CuO/Fe_2O_3 NPs plot was divided into three stages with three straight lines that did not pass through the origin, implying that the intra-particle diffusion process was not the only rate-controlling step in the bio-sorption process. For the first stage, CR dye in the aqueous solution was transferred to the surface of the bio-synthesized NPs (film diffusion). After that, at the second stage, the dye particles from external surface were transmigrated and bio-sorbed into the pores of the bio-synthesized NPs (intraparticle diffusion). The third stage was bio-sorption attachment of CR dye molecules [65, 66]. The linearized graphs of the four kinetic models were illustrated in Fig. 9 and their kinetic parameters are in Table 2.

Table 2: Kinetic Parameters of different kinetic models for bio-sorption of Congo Red onto the biosynthesized CuO\Fe_2O_3 NPs.

Kinetic Model		The biosynthesized CuO\Fe_2O_3 NPs
Pseudo-First-Order	q_e (mg/g) Calculated	3.4149
	q_e (mg/g) Experimental	48.804
	k_1 (min^{-1})	-0.01
	R^2	0.858
Pseudo-Second-Order	q_e (mg/g) Calculated	48.605
	q_e (mg/g) Experimental	48.804
	k_2 (g/mg min)	0.017
	R^2	0.998
Elovich	β (g/mg)	0.979
	$\dot{\alpha}$ (mg/g min)	43.167
	R^2	0.841
Intra-particle Diffusion	ki_d1	3.8017
	ki_d2	0.0618
	ki_d3	0.0407
	I	44.766
	R^2	0.612

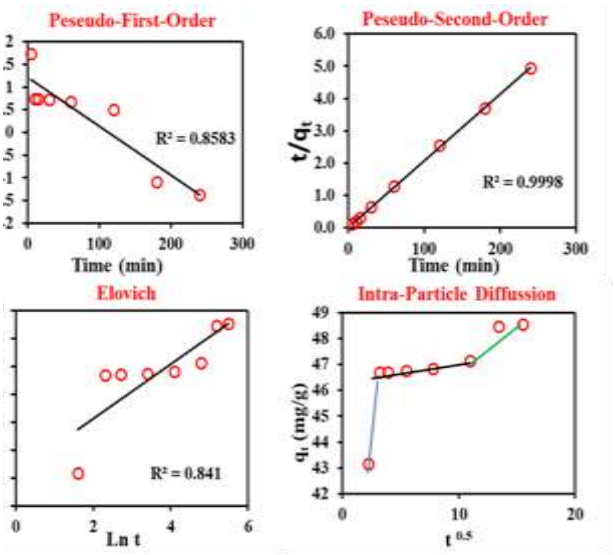

Figure (9): different kinetic models for bio-sorption of Methyl Blue onto the biosynthesized CuO\Fe_2O_3 NPs: First-order plots, Second-order plots, Elovich plots, and Intra-particle diffusion plots.

3.9. Equilibrium studies of Congo red dye bio-sorption onto the biosynthesized CuO\Fe₂O₃ NPs.

Equilibrium isotherms are widely used to determine whether the bio-sorption process of the bio-sorbate onto the bio-sorbent proceeds favorably, the type of bio-sorption, maximum capacity of bio-sorption, and the bio-sorption nature. Langmuir [67] and Freundlich [68] models which are two commonly used models were applied to the obtained data from bio-sorption studies. The Langmuir isotherm model assumes a monolayer bio-sorption that usually takes place on homogeneous surfaces and is expressed by the following equations:

$\frac{C_e}{q_e}$ =1/(q_(m) k)+ $\frac{C_e}{q_m}$

Where qe is the CR amount bio-sorbed at equilibrium (mg/g), qm is the maximum monolayer coverage capacities (mg/g), K is the Langmuir constant (L/mg), and Ce is the equilibrium concentration of CR (mg/L). Figure 9 showed a straight line with a high correlation coefficient value (R^2 = 0.952) for the linearized plot between (C_e/qe) verses (C_e/qm) of equation [40], the obtained parameters of the equation isotherm, qm values obtained from the plotted intercept, and the K_L values from the slope were tabulated in Table 3.

Table 3: Parameters of the applied bio-sorption isotherm mode

Isotherm parameters	The biosynthesized CuO/Fe_2O_3 NPs
Langmuir	
q_m (mg g−1) calculated	155.738
K_L (L mg^{-1})	0.106
R^2	**0.952**
Freundlich	
K_F ($mg1^{-1}$/n L1/n g^{-1})	3353.022
n_f	3.33
R^2	**0.897**

Subsequently, the Langmuir isotherm model was suitable to describe the bio-sorption process of CR dye onto the biosynthesized NPs. According to the obtained qm values (155.738 mg/g), it was so obvious the great ability of the bio-synthesized NPs to bio-sorb CR dye from aqueous solutions. Moreover, the K_L value of the isotherm constant is located between 0 and 1, indicating the advantageous bio-sorption of CR molecules onto the bio-synthesized NPs [69].

The Freundlich model assumes a heterogeneous and multi-layer of the bio-sorption process, and it is lack information about the monolayer bio-sorption capacity of bio-sorbent matrix, in contrast to the Langmuir model. The linearized form of the Freundlich equation may be expressed as:

$$\ln q_e = \ln k_{f+} \frac{1}{n_f} \ln C_e \qquad (5)$$

where q_e is the amount of CR dye bio-sorbed at equilibrium (mg/g); C_e is the concentration of the bio-synthesized NPs at equilibrium (mg/L); and K_f and n_f are Freundlich constants related to the bio-sorption capacity and intensity, respectively. The linear plot between lnCe and lnqe of the Freundlich equation was illustrated in Figure 10. The "n" values represent the slope of this plot, while the K_f values represent the intersection point, and they were tabulated in Table 3. The obtained "n" values from Freundlich isotherm were found between 1 and 10. Which means that the bio-sorption process was favorable. However, the obtained correlation coefficients were not high compared to the Langmuir (R^2= 0.897), indicating that, the Langmuir isotherm model is more fitted to describe CR dye onto the biosynthesized NPs than Freundlich. In other words, the bio-sorption process takes place in a single layer and on homogeneous surfaces and there is no transmigration of the dye molecules to the inner layer of the adsorbent [70, 71].

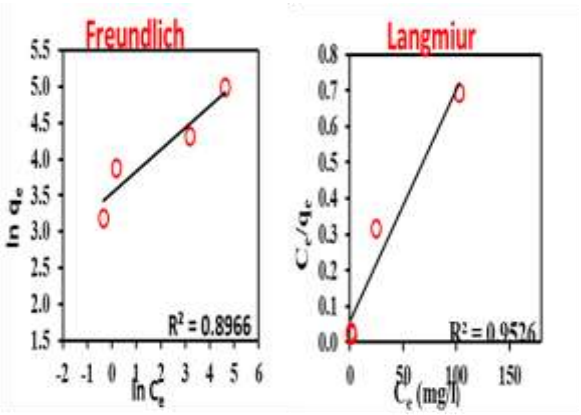

Figure (10): Equilibrium isotherm models (Freundlich and Langmuir) Congo red dye bio-sorption onto the biosynthesized CuO\Fe_2O_3 NPs.

3.10. Effect of initial Congo red concentration on its removal %

The influence of initial CR dye concentrations on its bio-sorption rate was investigated in the 25, 50, 100, and 250 mg/L concentration range at 150 rpm agitation speed and 0.1 g/L of the bio-synthesized NPs dosage (Fig.11). It was clear from the figure that the dye removal% was inversely proportional to its initial concentration, while the R% decreased from 97.167 to 58.985 % when the initial CR concentration increased from 25 up to 250 ppm, respectively. This might be since, at lower dye concentrations, there are high active sites ratio located on the bio-synthesized NPs to the number of dye molecules, and subsequently, the interactions between the dye molecules and the bio-sorbent are higher and as a result, the R% is higher [72].

However, as shown in the figure, when the initial CR concentration was increased from 25 to 250 ppm, the bio-sorption capacity increased from 24.292 mg/g to 147.463 mg/g. These outcomes might be explained by the fact that the availability of dye ions around the bio-synthesized NPs increases before reaching the adsorption-desorption equilibrium at higher concentrations of the dye, which in turn accelerates the dye diffusion because of the increase in the driving force of the concentration gradient for mass transfer [73, 74].

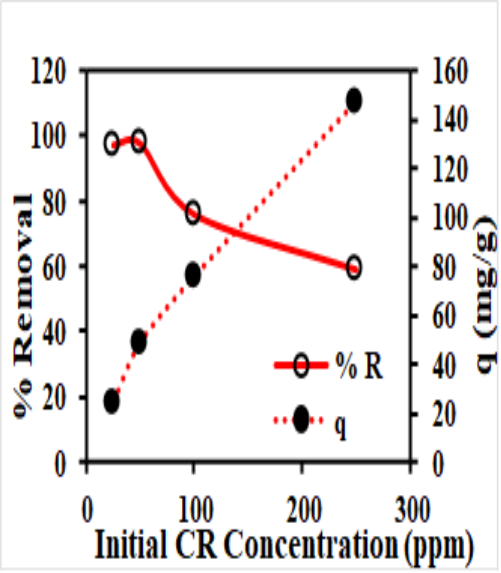

Figure (11): Effect of initial CR dye concentration on its removal percentage.

3.11. Optimization of Congo red removal using Central Composite Design (CCD)

The maximum removal of Congo red was obtained at 99.211%, where the optimal condition of Congo red sorption was obtained at 40 ppm of Congo red concentration, 2g\L of NPs dosage, 4 for pH and the contact time was 180 min.

Model selection was performed using backward feature selection based on a p-value threshold close to α=0.1 level. Starting with a quadratic model that includes all the linear and interaction terms the model is refined iteratively by removing the least significant term and refitting until no terms are above the desired threshold. The final selected model is in the table which is a reduced two factor interaction model (Table 4).

Table 4. ANOVA for Reduced 2FI model (R %)

Source	Sum of Squares	Df	Mean Square	F-value	p-value
Model	808.50	5	161.70	9.84	< 0.0001
A-dye	27.22	1	27.22	1.66	0.2104
C-pH	321.49	1	321.49	19.56	0.0002
D-Time	190.45	1	190.45	11.59	0.0023
AC	34.21	1	34.21	2.08	0.1620
CD	235.14	1	235.14	14.31	0.0009
Residual	394.38	24	16.43		
Lack of Fit	392.21	19	20.64	47.58	0.0002
Pure Error	2.17	5	0.4339		
Cor Total	1202.88	29			
Fit Statistics					
Std. Dev.	4.05		**R^2**	0.6721	
Mean	94.62		**Adjusted R^2**	0.6038	
C.V. %	4.28		**Adeq Precision**	11.1191	
Final Model Equation					
R % Fe\Cu NPs = +94.62 +1.06***A** -3.66***C** +2.82***D** +1.46***AC** +3.83***CD**					

The residual table contains the predictions obtained using the fitted model equation above for each data point and comparing it to the actual experimental values by taking the difference between them to get the residual (error) for the model (Table 5).

Table 5. Residual Table for (**R % Fe_2O_3\CuO NPs).**

Run Order	Actual Value	Predicted Value	Residual	Standard Order
1	96.66	94.62	2.04	19
2	98.11	98.90	-0.7909	4
3	97.65	92.49	5.16	17
4	96.83	100.13	-3.30	14

5	94.67	94.62	0.0514	26
6	94.05	94.62	-0.5676	29
7	95.98	94.62	1.36	28
8	96.27	95.08	1.19	13
9	95.20	95.08	0.1200	15
10	96.60	100.25	-3.65	24
11	98.33	99.69	-1.36	1
12	91.73	86.83	4.90	6
13	95.44	87.30	8.14	22
14	90.27	94.62	-4.35	20
15	99.21	96.86	2.35	10
16	79.33	86.83	-7.50	8
17	95.44	94.62	0.8234	25
18	75.67	81.78	-6.11	5
19	99.05	96.86	2.19	12
20	99.05	97.66	1.39	9
21	98.38	99.69	-1.31	3
22	75.33	81.78	-6.45	7
23	98.61	96.75	1.86	18
24	94.98	94.62	0.3604	27
25	98.81	97.66	1.15	11
26	98.95	101.94	-2.98	21
27	95.05	94.62	0.4374	30
28	98.32	98.90	-0.5729	2
29	96.44	88.98	7.46	23
30	98.08	100.13	-2.05	16

Predictions from each fitted linear model plotted against actual experimental values. The line represents perfect predictions and the distance of deviations represents the residual. CuO\Fe$_2$O$_3$ model predictions have a high skill with deviations along the entire line which matches the R^2 values visually (Figure 12).

Figure 12: The predicted response values versus the actual response values for CR removal using CuO\Fe$_2$O$_3$ NPs

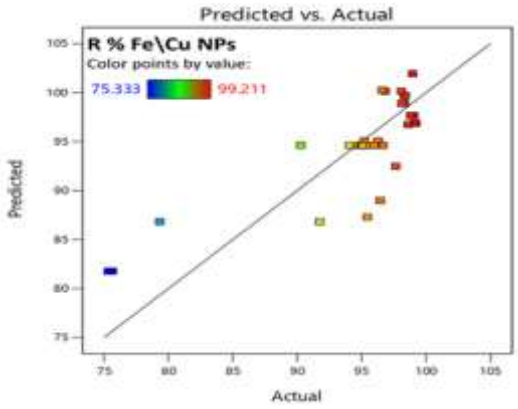

Fitted model predictions vs residual errors (difference from actual experimental values). CuO\Fe$_2$O$_3$ model residuals cluster closer to the zero line at higher values with 3 points not within 2 sigma at both higher and lower values (Figure 13).

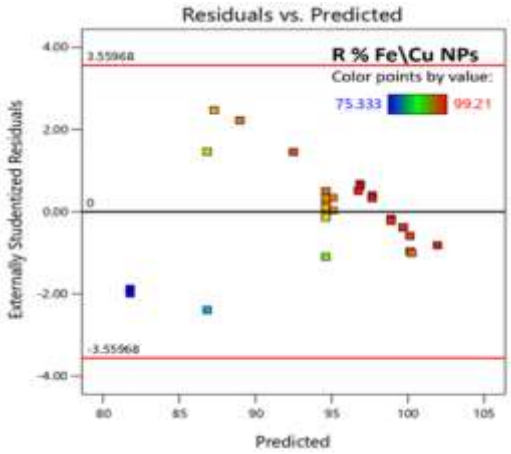

Figure 13: Predicted vs. normal residual errors plots of CR removal using CuO\Fe$_2$O$_3$ NP

The response surface for CuO\Fe$_2$O$_3$ is maximized using a Hill Climbing algorithm using the linear model and constraints from the experiment. 4 graphs are produced for the interactions between two factors while keeping the remaining two factors fixed at optimal levels and varying the others (Figure 14).

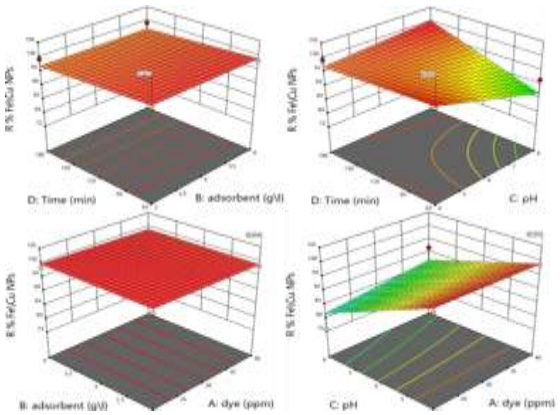

Figure 14: 3D Surface plots of CR removal using CuO\Fe$_2$O$_3$ NPs

3.12. Phytotoxicity study

Evaluation of *Vicia faba* Sakha1 seed germination response towards the Congo red hazards was carried out using the dye after and before treatments (Fig.15). There was 100% Germination in control dist water. The germination (%) of *Vicia faba* was found to be 100% with the treated dye while for the seeds that were treated with Congo dye, the percentage of germination was zero. The length of the shoot and root were affected by the untreated dyes more than the

treated ones. The growth parameters present in the fresh samples were higher than the dry ones (except the dry shoot length), that's because iron nanoparticles can penetrate the seed coat and promote the ability of water absorption and utilization, and improves germination. The plumule and radicle length of *Vicia faba* was represented in Table 6.

Figure (15): A) seed treated with dist water, B) seed treated with Congo red, C) seed treated with treated water

Table 6: Growth parameters of *Vicia faba* Sakha 1 after watering by treated Congo red.

Growth parameters	Control	Treated Congo Red	Percent of increase/decrease
Fresh shoot length	2.4 ± 0.518	3.5 ± 1.38	45.83
Dry shoot length	2.02 ± 0.35	2.13 ± 1.31	5.45
Fresh Shoot Weight	0.33± 0.084	0.45 ± 0.1	36.36
Dry Shoot Weight	0.057± 0.031	0.0497± 0.031	- 12.81
Fresh Root Length	5.2 ± 2.24	6.82 ± 2	31.15
Dry Root Length	3.9 ± 1.71	3.75 ± 1.33	- 3.85
Fresh Root Weight	0.388 ± 0.12	0.475 ± 0.25	22.42
Dry Root Weight	0.052 ± 0.036	0.028 ± 0.017	- 46.15

4. Conclusion

Copper\iron nanoparticles were successfully synthesized by using the cell extract of Fusarium oxysporum which is a cost-effective, eco-friendly method. The formation of $CuO\backslash Fe_2O_3$ nanoparticles was confirmed by using UV-Vis spectroscopy and the color change of the extract solution. FTIR spectrum proved that the biomolecules present in the fungal extract acted as a reducing and capping agent in the synthesis of $CuO\backslash Fe_2O_3$ nanoparticles. XRD spectra show the crystalline structure of mycosynthesized nanoparticles. The biosynthesized $CuO\backslash Fe_2O_3$ Nps has good antibacterial activity against both Gram-positive and Gram-negative bacteria. Congo red dye adsorption was studied by using mycosynthesized $CuO\backslash Fe_2O_3$ nanoparticles. Antibacterial activity and adsorption activity prove that $CuO\backslash Fe_2O_3$ nanoparticles have excellent applications in wastewater treatment.

5. Refrences

1. Ahmad, I.Z., A. Ahmad, H. Tabassum, and M. Kuddus, Applications of Nanoparticles in the Treatment of Wastewater. Handb. Ecomater., Springer, Cham, 2017: p. 1-25.
2. Gupta, V., Application of low-cost adsorbents for dye removal–a review. Journal of environmental management, 2009. **90**(8): p. 2313-2342.
3. Vidovix, T.B., H.B. Quesada, E.F.D. Januário, R. Bergamasco, and A.M.S. Vieira, Green synthesis of copper oxide nanoparticles using *Punica granatum* leaf extract applied to the removal of methylene blue. Materials Letters, 2019. **257**: p. 126685.
4. Kumari, P., M. Alam, and W.A. Siddiqi, Usage of nanoparticles as adsorbents for waste water treatment: an emerging trend. Sustainable Materials Technologies, 2019. **22**: p. e00128.
5. Manikandan, S., R. Subbaiya, M. Saravanan, M. Ponraj, M. Selvam, and A. Pugazhendhi, A critical review of advanced nanotechnology and hybrid membrane based water recycling, reuse, and wastewater treatment processes. Chemosphere, 2022. **289**: p. 132867.
6. Chauhan, G., R.B. González-González, and H.M. Iqbal, Bioremediation and decontamination potentials of metallic nanoparticles loaded nanohybrid matrices–a review. Environmental Research, 2022. **204**: p. 112407.
7. Ali, H., E. Khan, and I. Ilahi, Environmental chemistry and ecotoxicology of hazardous heavy metals: environmental persistence, toxicity, and bioaccumulation. Journal of chemistry, 2019. **2019**.
8. Chahal, S., N. Rani, A. Kumar, and P. Kumar, Electronic structure and photocatalytic activity of samarium doped cerium oxide nanoparticles for hazardous rose bengal dye degradation. Vacuum, 2020. **172**: p. 109075.
9. Naghizade Asl, M., N.M. Mahmodi, P. Teymouri, B. Shahmoradi, R. Rezaee, and A. Maleki,

Adsorption of organic dyes using copper oxide nanoparticles: isotherm and kinetic studies. Desalination Water Treatment, 2016. **57**(52): p. 25278-25287.
10. Ngoc, P.K., T.K. Mac, H.T. Nguyen, T.D. Thanh, P. Van Vinh, B.T. Phan, A.T. Duong, and R. Das, Superior organic dye removal by CoCr2O4 nanoparticles: adsorption kinetics and isotherm. Journal of Science: Advanced Materials Devices, 2022. **7**(2): p. 100438.
11. David, L. and B. Moldovan, Green synthesis of biogenic silver nanoparticles for efficient catalytic removal of harmful organic dyes. Nanomaterials, 2020. **10**(2): p. 202.
12. Sharif, H.M.A., A. Mahmood, H.-Y. Cheng, R. Djellabi, J. Ali, W.-L. Jiang, S.-S. Wang, M.R. Haider, N. Mahmood, and A.-J. Wang, Fe3O4 nanoparticles coated with EDTA and Ag nanoparticles for the catalytic reduction of organic dyes from wastewater. ACS Applied Nano Materials, 2019. **2**(8): p. 5310-5319.
13. Choi, H.-D., M.-C. Shin, D.-H. Kim, C.-S. Jeon, and K. Baek, Removal characteristics of reactive black 5 using surfactant-modified activated carbon. Desalination, 2008. **223**(1-3): p. 290-298.
14. Verma, A., Water Pollution: Sources, Control and Treatment Measures, in Basic Concepts in Environmental Biotechnology. 2021, CRC Press. p. 35-44.
15. Kumar, S., S. Yadav, N. Kataria, A.K. Chauhan, S. Joshi, R. Gupta, P. Kumar, J.W.R. Chong, K.S. Khoo, and P.L. Show, Recent Advancement in Nanotechnology for the Treatment of Pharmaceutical Wastewater: Sources, Toxicity, and Remediation Technology. Current Pollution Reports, 2023: p. 1-33.
16. Jain, R. and S. Sikarwar, Photocatalytic and adsorption studies on the removal of dye Congo red from wastewater. International journal of environment pollution
2006. **27**(1-3): p. 158-178.
17. Chatterjee, S., N. Guha, S. Krishnan, A.K. Singh, P. Mathur, and D.K. Rai, Selective and recyclable Congo red dye adsorption by spherical Fe3O4 nanoparticles functionalized with 1, 2, 4, 5-benzenetetracarboxylic acid. Scientific reports, 2020. **10**(1): p. 111.
18. Khedr, M., K.A. Halim, and N. Soliman, Synthesis and photocatalytic activity of nano-sized iron oxides. Materials Letters, 2009. **63**(6-7): p. 598-601.
19. Andualem, W.W., F.K. Sabir, E.T. Mohammed, H.H. Belay, and B.A. Gonfa, Synthesis of copper oxide nanoparticles using plant leaf extract of *Catha edulis* and its antibacterial activity. Journal of Nanotechnology, 2020. **2020**: p. 1-10.
20. Sathiyavimal, S., S. Vasantharaj, V. Veeramani, M. Saravanan, G. Rajalakshmi, T. Kaliannan, F.A. Al-Misned, and A. Pugazhendhi, Green chemistry route of biosynthesized copper oxide nanoparticles using *Psidium guajava* leaf extract and their antibacterial activity and effective removal of industrial dyes. Journal of Environmental Chemical Engineering, 2021. **9**(2): p. 105033.
21. Jamzad, M. and M. Kamari Bidkorpeh, Green synthesis of iron oxide nanoparticles by the aqueous extract of *Laurus nobilis* L. leaves and evaluation of the antimicrobial activity. Journal of Nanostructure in Chemistry, 2020. **10**: p. 193-201.
22. Madubuonu, N., S.O. Aisida, I. Ahmad, S. Botha, T.-k. Zhao, M. Maaza, and F.I. Ezema, Bio-inspired iron oxide nanoparticles using *Psidium guajava* aqueous extract for antibacterial activity. Applied Physics A, 2020. **126**: p. 1-8.
23. Shkodenko, L., I. Kassirov, and E. Koshel, Metal oxide nanoparticles against bacterial biofilms: Perspectives and limitations. Microorganisms, 2020. **8**(10): p. 1545.
24. Haider, A., M. Ijaz, M. Imran, M. Naz, H. Majeed, J. Khan, M. Ali, and M. Ikram, Enhanced bactericidal action and dye degradation of spicy roots' extract-incorporated fine-tuned metal oxide nanoparticles. Applied Nanoscience, 2020. **10**: p. 1095-1104.
25. Menazea, A. and M. Ahmed, Silver and copper oxide nanoparticles-decorated graphene oxide via pulsed laser ablation technique: Preparation, characterization, and photoactivated antibacterial activity. Nano-Structures Nano-Objects, 2020. **22**: p. 100464.
26. Darezereshki, E., M. Ranjbar, and F. Bakhtiari, One-step synthesis of maghemite (γ-Fe2O3) nano-particles by wet chemical method. Journal of Alloys Compounds, 2010. **502**(1): p. 257-260.
27. Khan, S., S. Mansoor, Z. Rafi, B. Kumari, A. Shoaib, M. Saeed, S. Alshehri, M.M. Ghoneim, M. Rahamathulla, and U. Hani, A review on nanotechnology: Properties, applications, and mechanistic insights of cellular uptake mechanisms. Journal of Molecular Liquids, 2022. **348**: p. 118008.
28. Dheyab, M.A., A.A. Aziz, M.S. Jameel, and N. Oladzadabbasabadi, Recent advances in synthesis, modification, and potential application of tin oxide nanoparticles. Surfaces Interfaces, 2022. **28**: p. 101677.
29. Zhang, X., S. Yan, R. Tyagi, and R. Surampalli, Synthesis of nanoparticles by microorganisms and their application in enhancing microbiological reaction rates. Chemosphere, 2011. **82**(4): p. 489-494.

30. Mughal, B., S.Z.J. Zaidi, X. Zhang, and S.U. Hassan, Biogenic nanoparticles: Synthesis, characterisation and applications. Applied Sciences, 2021. **11**(6): p. 2598.
31. Sanchis-Gual, R., M. Coronado-Puchau, T. Mallah, and E. Coronado, Hybrid nanostructures based on gold nanoparticles and functional coordination polymers: Chemistry, physics and applications in biomedicine, catalysis and magnetism. Coordination Chemistry Reviews, 2023. **480**: p. 215025.
32. Shafey, A.M.E., Green synthesis of metal and metal oxide nanoparticles from plant leaf extracts and their applications: A review. Green Processing Synthesis, 2020. **9**(1): p. 304-339.
33. He, K., G. Chen, G. Zeng, Z. Huang, Z. Guo, T. Huang, M. Peng, J. Shi, and L. Hu, Applications of white rot fungi in bioremediation with nanoparticles and biosynthesis of metallic nanoparticles. Applied Microbiology Biotechnology, 2017. **101**(12): p. 4853-4862.
34. Ikram, M., J. Hassan, A. Raza, A. Haider, S. Naz, A. Ul-Hamid, J. Haider, I. Shahzadi, U. Qamar, and S. Ali, Photocatalytic and bactericidal properties and molecular docking analysis of TiO 2 nanoparticles conjugated with Zr for environmental remediation. RSC advances, 2020. **10**(50): p. 30007-30024.
35. Zhu, Y., X. Liu, Y. Hu, R. Wang, M. Chen, J. Wu, Y. Wang, S. Kang, Y. Sun, and M. Zhu, Behavior, remediation effect and toxicity of nanomaterials in water environments. Environmental research, 2019. **174**: p. 54-60.
36. Jadoun, S., R. Arif, N.K. Jangid, and R.K. Meena, Green synthesis of nanoparticles using plant extracts: A review. Environmental Chemistry Letters, 2021. **19**: p. 355-374.
37. Zhang, D., X.-l. Ma, Y. Gu, H. Huang, and G.-w. Zhang, Green synthesis of metallic nanoparticles and their potential applications to treat cancer. Frontiers in Chemistry, 2020. **8**: p. 799.
38. Pal, G., P. Rai, and A. Pandey, Green synthesis of nanoparticles: A greener approach for a cleaner future, in Green synthesis, characterization and applications of nanoparticles. 2019, Elsevier. p. 1-26.
39. Gebre, S.H. and M.G. Sendeku, New frontiers in the biosynthesis of metal oxide nanoparticles and their environmental applications: an overview. SN Applied Sciences, 2019. **1**(8): p. 1-28.
40. Eldeghidy, A., G. Abdel-Fattah, H. Aldesuquy, and A. Elsayed, GREEN SYNTHESIS AND CHARACTERIZATION OF NANO-IRON PARTICLES BY *Fusaium oxysporum* Running title: Nanparticles from fungi.
41. Elsayed, A., G.M. El-Shamy, and A.A. Attia, Biosynthesis, Characterization, and Assessment of Zirconia Nanoparticles by *Fusarium oxysporum* species as Potential Novel Antimicrobial and Cytotoxic Agents. Egyptian Journal of Botany, 2022. **62**(2): p. 507-522.
42. Soliman, H., A. Elsayed, and A. Dyaa, Antimicrobial activity of silver nanoparticles biosynthesised by Rhodotorula sp. strain ATL72. Egyptian Journal of Basic Applied Sciences, 2018. **5**(3): p. 228-233.
43. Elsayed, A., K. Hashish, and A.-D.J.J.o.E.S. Sherief, Production and characterization OF silver nanoparticles synthesized BY nanoparticles synthesized BY *FUSARIUM oxysporum FUSARIUM oxysporum.* 2015. **44**(4): p. 681-691.
44. He, M.Q., Y. Ai, W. Hu, L. Guan, M. Ding, and Q. Liang, Recent Advances of Seed-Mediated Growth of Metal Nanoparticles: from Growth to Applications. Advanced Materials, 2023: p. 2211915.
45. Saleem, S., M.H. Jameel, N. Akhtar, N. Nazir, A. Ali, A. Zaman, A. Rehman, S. Butt, F. Sultana, and M. Mushtaq, Modification in structural, optical, morphological, and electrical properties of zinc oxide (ZnO) nanoparticles (NPs) by metal (Ni, Co) dopants for electronic device applications. Arabian Journal of Chemistry, 2022. **15**(1): p. 103518.
46. Chari, N., L. Felix, M. Davoodbasha, A.S. Ali, and T. Nooruddin, In vitro and in vivo antibiofilm effect of copper nanoparticles against aquaculture pathogens. Biocatalysis agricultural biotechnology, 2017. **10**: p. 336-341.
47. Demirezen, D.A., Y.Ş. Yıldız, Ş. Yılmaz, and D.D. Yılmaz, Green synthesis and characterization of iron oxide nanoparticles using *Ficus carica* (common fig) dried fruit extract. Journal of bioscience bioengineering, 2019. **127**(2): p. 241-245.
48. Pugazhendhi, A., T.N.J.I. Edison, I. Karuppusamy, and B. Kathirvel, Inorganic nanoparticles: a potential cancer therapy for human welfare. International journal of pharmaceutics, 2018. **539**(1-2): p. 104-111.
49. Saratale, R.G., I. Karuppusamy, G.D. Saratale, A. Pugazhendhi, G. Kumar, Y. Park, G.S. Ghodake, R.N. Bharagava, J.R. Banu, and H.S. Shin, A comprehensive review on green nanomaterials using biological systems: Recent perception and their future applications. Colloids Surfaces B: Biointerfaces, 2018. **170**: p. 20-35.
50. Ren, Y., Y. Yuan, B. Lai, Y. Zhou, and J. Wang, Treatment of reverse osmosis (RO) concentrate by the combined Fe/Cu/air and Fenton process (1stFe/Cu/air-Fenton-2ndFe/Cu/air). Journal of hazardous materials, 2016. **302**: p. 36-44.
51. Ye, J., Y. Wang, Q. Xu, H. Wu, J. Tong, and J. Shi, Removal of hexavalent chromium from

wastewater by Cu/Fe bimetallic nanoparticles. Scientific Reports, 2021. **11**(1): p. 10848.
52. Bakina, O., E. Glazkova, N. Svarovskaya, N. Rodkevich, and M. Lerner, «Janus»-like Cu-Fe bimetallic nanoparticles with high antibacterial activity. Materials letters, 2019. **242**: p. 187-190.
53. Ramírez Calderón, O.A., O.M. Abdeldayem, A. Pugazhendhi, and E.R. Rene, Current updates and perspectives of biosorption technology: an alternative for the removal of heavy metals from wastewater. Current Pollution Reports, 2020. **6**(1): p. 8-27.
54. Alavi, M. and M. Rai, Recent advances in antibacterial applications of metal nanoparticles (MNPs) and metal nanocomposites (MNCs) against multidrug-resistant (MDR) bacteria. Expert review of anti-infective therapy, 2019. **17**(6): p. 419-428.
55. El-Sesy, M.E. and S.A. Othman, Promising antibacterial activities of anethole and green-synthesized magnetite nanoparticles against multiple antibiotic-resistant bacteria. Water Science Technology, 2023. **87**(3): p. 729-747.
56. Elekhnawy, E., F. Sonbol, A. Abdelaziz, and T. Elbanna, Potential impact of biocide adaptation on selection of antibiotic resistance in bacterial isolates. Future Journal of Pharmaceutical Sciences, 2020. **6**(1): p. 1-10.
57. Ali, I., T.Y. Qiang, N. Ilahi, M. Adnan, and W. Sajjad, Green synthesis of silver nanoparticles by using bacterial extract and its antimicrobial activity against pathogens. Int J Biosci, 2018. **13**(5): p. 1-5.
58. Marcato, P., G. De Souza, O. Alves, E. Esposito, and N. Durán, Antibacterial activity of silver nanoparticles synthesized by *Fusarium oxysporum* strain. Proceedings of 2nd Mercosur Congr. on Chem. Eng., 4th Mercosur Congr. on Process Sys. Eng, 2005: p. 1-5.
59. Ugraskan, V., B. Isik, and O. Yazici, Adsorptive removal of methylene blue from aqueous solutions by porous boron carbide: isotherm, kinetic and thermodynamic studies. Chemical Engineering Communications, 2022. **209**(8): p. 1111-1129.
60. Zainith, S., D. Purchase, G.D. Saratale, L.F.R. Ferreira, M. Bilal, and R.N. Bharagava, Isolation and characterization of lignin-degrading bacterium *Bacillus aryabhattai* from pulp and paper mill wastewater and evaluation of its lignin-degrading potential. 3 Biotech, 2019. **9**(3): p. 1-11.
61. El-Kady, M., M. El-Aassar, O.A. El Batrawy, M.S. Ibrahim, H.S. Hassan, and H. Fakhry, Equilibrium and Kinetic Behaviors of Cationic Dye Decolorization Using Poly (AN-co-Py)/ZrO_2 Novel Nanopolymeric Composites. Advances in Polymer Technology, 2018. **37**(3): p. 740-752.
62. Fakhry, H., H. Hassan, M. El-Aassar, I.H. Alsohaimi, M.F. Hussein, M.M. ALQahtani, and Y.A. El-Amier, A Treatment of Wastewater Containing Safranin O Using Immobilized Myriophyllum spicatum L. onto Polyacrylonitrile/Polyvinylpyrrodlidone Biosorbent. Journal of Inorganic Organometallic Polymers Materials, 2022: p. 1-15.
63. Fakhry, H., M. El-Sonbati, B. Omar, R. El-Henawy, Y. Zhang, and E.-K. Marwa, Novel fabricated low-cost hybrid polyacrylonitrile/polyvinylpyrrolidone coated polyurethane foam (PAN/PVP@ PUF) membrane for the decolorization of cationic and anionic dyes. Journal of Environmental Management, 2022. **315**: p. 115128.
64. El-Amier, Y.A., A. Elsayed, M.A. El-Esawi, A. Noureldeen, H. Darwish, and H. Fakhry, Optimizing the biosorption behavior of Ludwigia stolonifera in the removal of lead and chromium metal ions from synthetic wastewater. Sustainability, 2021. **13**(11): p. 6390.
65. Somsesta, N., V. Sricharoenchaikul, and D. Aht-Ong, Adsorption removal of methylene blue onto activated carbon/cellulose biocomposite films: equilibrium and kinetic studies. Materials chemistry physics, 2020. **240**: p. 122221.
66. Ma, X., C. Liu, D.P. Anderson, and P.R. Chang, Porous cellulose spheres: Preparation, modification and adsorption properties. Chemosphere, 2016. **165**: p. 399-408.
67. Langmuir, I., The adsorption of gases on plane surfaces of glass, mica and platinum. Journal of the American Chemical society, 1918. **40**(9): p. 1361-1403.
68. Freundlich, H., Über die adsorption in lösungen. Zeitschrift für physikalische Chemie, 1907. **57**(1): p. 385-470.
69. Zhao, X., X. Wang, and T. Lou, Preparation of fibrous chitosan/sodium alginate composite foams for the adsorption of cationic and anionic dyes. Journal of Hazardous Materials, 2021. **403**: p. 124054.
70. Jawad, A.H., S. Sabar, M.A.M. Ishak, L.D. Wilson, S.S. Ahmad Norrahma, M. Talari, and A.M. Farhan, Microwave-assisted preparation of mesoporous-activated carbon from coconut (*Cocos nucifera*) leaf by H3PO4 activation for methylene blue adsorption. Chemical Engineering Communications, 2017. **204**(10): p. 1143-1156.
71. Bayramoglu, G. and M.Y. Arica, Removal of reactive dyes from wastewater by acrylate polymer beads bearing amino groups: isotherm and kinetic studies. Coloration Technology, 2013. **129**(2): p. 114-124.

72. Kumar, P.S., S. Ramalingam, and K. Sathishkumar, Removal of methylene blue dye from aqueous solution by activated carbon prepared from cashew nut shell as a new low-cost adsorbent. Korean Journal of chemical engineering, 2011. **28**(1): p. 149-155.
73. Hamzezadeh, A., Y. Rashtbari, S. Afshin, M. Morovati, and M. Vosoughi, Application of low-cost material for adsorption of dye from aqueous solution. International Journal of Environmental Analytical Chemistry, 2022. **102**(1): p. 254-269.
74. Deng, H., J. Lu, G. Li, G. Zhang, and X. Wang, Adsorption of methylene blue on adsorbent materials produced from cotton stalk. Chemical engineering journal, 2011. **172**(1): p. 326-334.